Light transport in $\mathcal{PT}$-invariant photonic structures with hidden symmetries

M. H. Teimourpour and R. El-Ganainy*
Department of Physics, Michigan Technological University, Houghton, Michigan 49931, USA

A. Eisfeld
Max Planck Institute for the Physics of Complex Systems, Nothnitzer Street 38, 01178 Dresden, Germany

A. Szameit
Institute of Applied Physics, Abbe School of Photonics, Friedrich Schiller University, Max-Wien-Platz 1, D-07743 Jena, Germany

D. N. Christodoulides
College of Optics & Photonics – CREOL, University of Central Florida, Orlando, Florida 32816, USA
(Received 16 May 2014; published 10 November 2014)

We introduce a recursive bosonic quantization technique for generating classical parity-time ($\mathcal{PT}$) photonic structures that possess hidden symmetries and higher-order exceptional points. We study light transport in these geometries and we demonstrate that perfect state transfer is possible only for certain initial conditions. Moreover, we show that for the same propagation direction, left and right coherent transports are not symmetric with field amplitudes following two different trajectories. A general scheme for identifying the conservation laws in such $\mathcal{PT}$-symmetric photonic networks is also presented.

DOI: 10.1103/PhysRevA.90.053817 PACS number(s): 42.25.Fx, 42.82.Et, 42.25.Hz

I. INTRODUCTION

Parity-time ($\mathcal{PT}$) symmetry in quantum mechanics has been a subject of intense investigations in the past decade. This interest was sparked by the seminal work of Bender and Boettcher [1] in which they demonstrated that a certain class of $\mathcal{PT}$-symmetric Hamiltonians can exhibit entirely real eigenvalue spectra. Within the context of a single-particle Schrodinger equation, $\mathcal{PT}$ symmetry arises from complex potentials having even (odd) symmetry for their real (imaginary) components [1–4]. Above a specific threshold for the imaginary part of the complex potential, the system experiences an abrupt phase transition where some real eigenvalues branch over to the complex plane, signaling the onset of spontaneous $\mathcal{PT}$ symmetry breaking [1–4]. These phase transition thresholds, also known as exceptional points [5,6], are marked by the coalescing of two or more eigenvectors.

The notion of $\mathcal{PT}$ symmetry was later extended to optical waveguide systems with complex refractive index profiles [7–9]. Similar to their quantum-mechanical counterparts, the real and imaginary components of the optical indices in these arrangements are even and odd functions, respectively [7–12]. $\mathcal{PT}$ symmetry in complex Bragg gratings [13] and optical cavities [14] has also been studied. In addition, non-Hermitian optical diodes have been proposed [15]. Within the context of coupled optical structures, $\mathcal{PT}$ symmetry has been mainly investigated in uniform lattices [8–10]. Nevertheless, very recently J_x arrays [16] exhibiting $\mathcal{PT}$ symmetry have been considered and their spectra were calculated using angular momentum operator algebra [17]. The dynamical properties of these $\mathcal{PT}$ coupled structures were also investigated and it was shown that they exhibit half-cycle conditional perfect state transfer (PST) below $\mathcal{PT}$ phase transition [18].

In this work we introduce a recursive bosonic quantization (RBQ) technique for generating new classes of $\mathcal{PT}$-symmetric networks that exhibit nonlinear topology and possess hidden symmetry. The latter property gives rise to spectral degeneracies that persist even above $\mathcal{PT}$ spontaneous symmetry breaking. We also investigate light transport in these geometries and we demonstrate that perfect state transfer is possible only for certain initial conditions. Moreover, we show that this coherent transport follows different trajectories in opposite directions. Finally, we present a scheme for finding the constants of motion in these configurations. It is important to note that even though we employ second quantization in our analysis, the investigated system is by no means quantum mechanical. In other words, we apply bosonic algebra only as a mathematical generator for higher-order *classical* $\mathcal{PT}$-symmetric arrays.

II. RECURSIVE SECOND QUANTIZATION AS A GENERATOR OF $\mathcal{PT}$ SYMMETRIC NETWORKS

We first start by considering a noninteracting $\mathcal{PT}$-symmetric two-site Bose-Hubbard Hamiltonian:

$$\hat{H}_2^{(1)} = -i\hbar\frac{\gamma}{2}(\hat{a}_1^\dagger\hat{a}_1 - \hat{a}_2^\dagger\hat{a}_2) + \hbar\kappa\,(\hat{a}_1^\dagger\hat{a}_2 + \hat{a}_1\hat{a}_2^\dagger). \tag{1}$$

Here $\hat{a}_{1,2}^\dagger$ and $\hat{a}_{1,2}$ are the bosonic creation and annihilation operators of sites 1 and 2, respectively, and they obey $[\hat{a}_i,\hat{a}_j] = [\hat{a}_i^\dagger,\hat{a}_j^\dagger] = 0, [\hat{a}_i,\hat{a}_j^\dagger] = \delta_{ij}$ where δ_{ij} is the Kronecker δ function. The parameter γ represents the gain or loss factor, while κ is the hopping constant between the two sites. Finally, the superscript in $\hat{H}_2^{(1)}$ indicates that this Hamiltonian was obtained by quantizing the classical $\mathcal{PT}$ coupled waveguide/cavity structures (i.e., it is the first step in an iterative process that will be explained later), while the subscript denotes the number of sites. The eigenvalue spectrum of Eq. (1) can be obtained in closed form by diagonalizing $\hat{H}_2^{(1)}$

*ganainy@mtu.edu

through the transformations $\begin{pmatrix}\hat{b}_e\\ \hat{b}_o\end{pmatrix}=\begin{pmatrix}\cos(\alpha/2) & \sin(\alpha/2)\\ -\sin(\alpha/2) & \cos(\alpha/2)\end{pmatrix}\begin{pmatrix}\hat{a}_1\\ \hat{a}_2\end{pmatrix}$ with $\tan(\alpha)=\frac{2\kappa}{i\gamma}$. By doing so, we obtain

$$\lambda_{M,m}=(M-2m)\,\hbar\sqrt{\kappa^2-(\gamma/2)^2},\quad m=0,1,2,\ldots,M, \tag{2}$$

where $\lambda_{M,m}$ are the eigenvalues associated with stationary states having m and $M-m$ bosons populating the even (odd)-like modes, respectively. Note that the spectrum $\lambda_{M,m}$ has one exceptional point of order M at $\gamma=2\kappa$. Without any loss of generality, we consider the case of $M=2N$ and employ the symmetrized bases $|n_{2N}\rangle=\frac{(\hat{a}_1^\dagger)^{N-n}(\hat{a}_2^\dagger)^{N+n}}{\sqrt{(N-n)!\,(N+n)!}}|\text{vac}\rangle=|N-n,N+n\rangle$, with $N\mp n$ being the number of bosons in sites 1 and 2, respectively, and $|\text{vac}\rangle$ is the vacuum state. In contrast to quantum systems, these bases are used here only to generate $\mathcal{PT}$-symmetric arrays and thus both integers and half integers are valid choices for N. The dynamical evolution of any arbitrary wavefunction inside this subspace is given by $|\psi(t)\rangle=\sum_{n=-N}^{N}c_n(t)\,|n_{2N}\rangle$, where the time-dependent amplitudes $c_n(t)$ are completely determined by their initial conditions $c_n(0)$ and the coupled ordinary differential equations (ODEs):

$$i\frac{d\vec{c}}{dt}=\Omega\,\vec{c},$$

$$\Omega=\begin{bmatrix}-i\gamma\,N & \kappa\,g_{-N+1} & & & \\ \cdots & \cdots & \cdots & \cdots & \cdots \\ & \kappa\,g_n & i\gamma\,n & \kappa\,g_{n+1} & \\ \cdots & \cdots & \cdots & \cdots & \cdots \\ & & & \kappa\,g_N & i\gamma\,N\end{bmatrix}, \tag{3}$$

where Ω is a tridiagonal matrix and $\vec{c}=[c_{-N}\ \cdots\ c_{N-1}\ c_N]^T$, with the superscript T indicating a matrix transpose. In Eq. (3), the coupling coefficients are symmetric around $n=0$ and are given by $g_n=\sqrt{(N+n)(N-n+1)}$. On the other hand, as expected the gain (loss) profile (determined by the diagonal elements of Ω) is antisymmetric and the system exhibits $\mathcal{PT}$ symmetry. These results were also obtained previously using angular momentum operator algebra [17,18]. Before we proceed, we would like to emphasize again that despite the quantum-mechanical origin of the problem, Eq. (3) is a system of ODEs that can be simulated optically by classical light transport in coupled waveguide or cavity arrays. For example, Figs. 1(a) and 1(b) depict a schematic of waveguide (cavity) arrays that can be used to emulate Eq. (3) when $N=1$ and $N=3/2$, respectively. The waveguides (cavities) are represented by the nodes, and the network connectivity (diagonal and off-diagonal values of Ω) is indicated in the figure. These structures can be realized using current photonic technology. For instance, the Hermitian analog of the arrays in Fig. 1 was experimentally investigated in optical waveguide lattices [16]. Moreover, $\mathcal{PT}$-symmetric optical waveguides, optical mesh periodic potentials, photonic arrays, and microcavities were also experimentally investigated [11,12,19–21].

Next, we show that more complicated $\mathcal{PT}$-symmetric networks (with nonlinear topologies) can be generated by successive application of the aforementioned bosonic

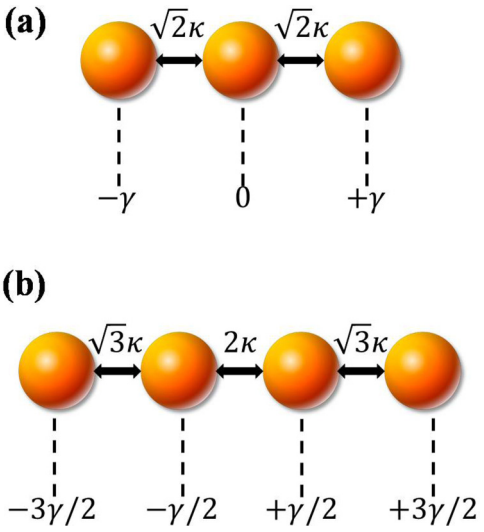

FIG. 1. (Color online) (a, b) A schematic of waveguide (cavity) arrays that can be used to emulate Eq. (3) when $N=1$ and $N=3/2$, respectively. The waveguides (cavities) are represented by the nodes, and the network connectivity [diagonal (off-diagonal) values of Ω] is indicated in the figure. Distances between elements are not shown to scale.

quantization procedure. As we will see, these structures exhibit an even richer spectral features than those generated from $\hat{H}_2^{(1)}$. We do so by replacing the c numbers c_n in Eq. (3) by a bosonic annihilation operator $\hat{a}_n$:

$$i\frac{d\vec{\hat{a}}}{dt}=\Omega\,\vec{\hat{a}}, \tag{4}$$

where $\vec{a}=[\hat{a}_{-N}\ \cdots\ \hat{a}_n\ \cdots\ \hat{a}_N]^T$ and the formal solution of Eq. (4) is given by $\vec{\hat{a}}\,(t)=\exp(-i\Omega\,t)\,\vec{\hat{a}}(0)$. In order to proceed, we note that Eq. (4) is the Heisenberg equation of motion associated with the Hamiltonian:

$$\hat{H}_{2N+1}^{(2)}=i\gamma\,\hbar\sum_{n=-N}^{N}n\,\hat{a}_n^\dagger\hat{a}_n + \kappa\,\hbar\left(\sum_{n=-N+1}^{N}g_n\hat{a}_n^\dagger\hat{a}_{n-1}+\sum_{n=-N}^{N-1}g_{n+1}\hat{a}_n^\dagger\hat{a}_{n+1}\right). \tag{5}$$

Finally, expanding $\hat{H}_{2N+1}^{(2)}$ in its Fock space generates higher-hierarchy $\mathcal{PT}$-symmetric structures. This recursive second quantization can be applied indefinitely to generate a higher hierarchy of complex $\mathcal{PT}$-symmetric networks.

III. $\mathcal{PT}$-SYMMETRIC STRUCTURES WITH HIDDEN SYMMETRY

We elaborate on the results of the previous section and we discuss the hidden symmetry associated with the construction of our iterative method by considering specific examples. More specifically, the second quantization of the $\mathcal{PT}$-symmetric configuration of Fig. 1(a) is given by $\hat{H}_3^{(2)}=-i\gamma\,\hbar(\hat{a}_1^\dagger\hat{a}_1-\hat{a}_3^\dagger\hat{a}_3)+\sqrt{2}\kappa\,\hbar(\hat{a}_1^\dagger\hat{a}_2+\hat{a}_1\hat{a}_2^\dagger+\hat{a}_2^\dagger\hat{a}_3+\hat{a}_2\hat{a}_3^\dagger)$.

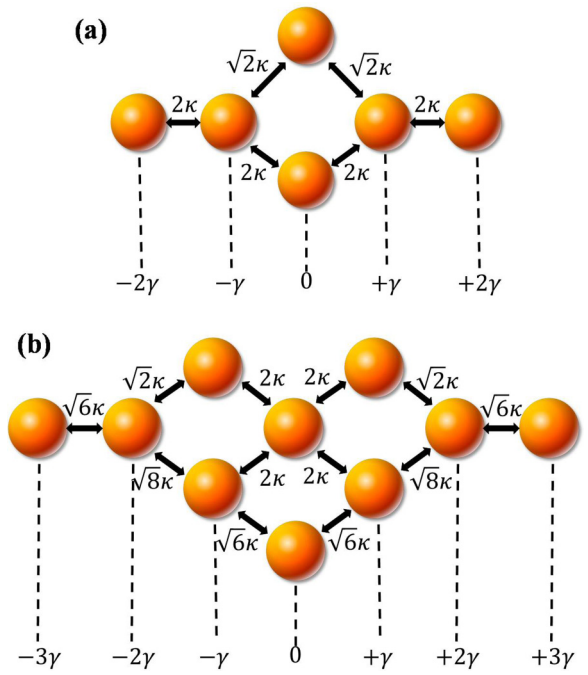

FIG. 2. (Color online) A schematic of the coupled photonic structures that correspond to two- and three-boson representations of $\hat{H}_3^{(2)}$ are shown in (a) and (b), respectively. Similar to Fig. 1, the diagonal and off-diagonal elements are also indicated in the figure. Distances between elements are not shown to scale.

As before, the Hamiltonian $\hat{H}_3^{(2)}$ can be also diagonalized by means of linear transformations and its eigenvalue spectrum is given by $\lambda_{M,m_1,m_2} = 2(M - 2m_1 - m_2)\hbar\sqrt{\kappa^2 - (\gamma/2)^2}, m_{1,2} = 0,1,2,\ldots,M$ with the condition $m_1 + m_2 \leqslant M$. Here $m_{1,2}$ are the occupation numbers of the two lowest supermodes of $H_3^{(2)}$, while $M - m_1 - m_2$ represents the population of the third mode. The two- and three-boson representations of $\hat{H}_3^{(2)}$ are shown in Figs. 2(a) and 2(b), correspondingly. In contrast to those shown in Fig. 1, we note that the $\mathcal{PT}$-symmetric networks depicted in Fig. 2 exhibit nonlinear topology. Together with the structure of the Hamiltonian, this leads to several intriguing features in the eigenvalue spectrum. More specifically, the $\mathcal{PT}$-symmetric array depicted in Fig. 2(a) has two degenerate eigenmodes associated with the stationary states $|1,0,1\rangle_D$ and $|0,2,0\rangle_D$, where the subscript D indicates a representation in the diagonal bases (where the numbers represent the occupation of the system's supermodes) as opposed to those defined by the site numbers. Moreover, these degenerate modes have a null eigenvalue, and they never undergo $\mathcal{PT}$ phase transitions, regardless of the values of γ. On the other hand, the network depicted in Fig. 2(b) exhibits even multiple sets of degenerate eigenstates. Similar to that of Fig. 2(a), the supermodes corresponding to the states $|1,1,1\rangle_D$ and $|0,3,0\rangle_D$ have zero eigenvalue and they never experience $\mathcal{PT}$ phase transition. On the other hand, each of the two sets of eigenstates $\{|0,2,1\rangle_D, |1,0,2\rangle_D\}$ and $\{|1,2,0\rangle_D, |2,0,1\rangle_D\}$ is doubly degenerate and their eigenvalues are complex conjugate. Higher-order symmetries can also be found in higher-hierarchy networks.

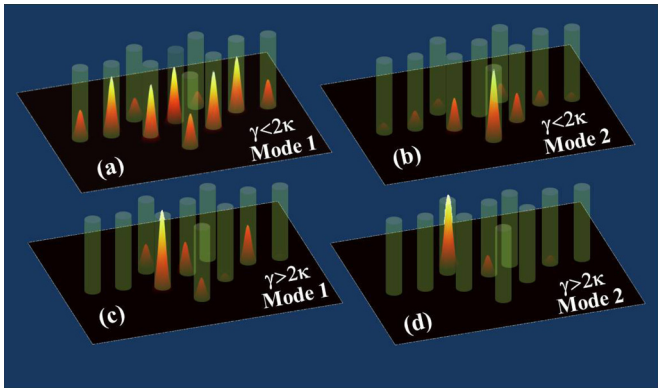

FIG. 3. (Color online) (a, b) The intensity distribution (or probability amplitudes) $|c_n|^2$ associated with the degenerate eigenmodes $|1,0,2\rangle_D$ and $|0,2,1\rangle_D$ when $\kappa = 1$ and $\gamma = 1$, while (c) and (d) illustrate the same modes when $\kappa = 1$ and $\gamma = 3$. Note that the onset of $\mathcal{PT}$ phase transition is $\gamma = 2\kappa$. The transparent cylinders represent the waveguide structure.

Figure 3 illustrates the intensity distribution (or probability amplitudes) $|c_n|^2$ associated with the degenerate eigenmodes $|1,0,2\rangle_D$ and $|0,2,1\rangle_D$ of the structure in Fig. 2(b). More specifically, the eigensolutions associated with the $\mathcal{PT}$-symmetric phase ($\gamma < 2\kappa$) are shown in Figs. 3(a) and 3(b), while the broken phase scenario is depicted in Figs. 3(c) and 3(d). It is remarkable that these degeneracies persist even when the $\mathcal{PT}$ symmetry is spontaneously broken. This fact is manifested in Figs. 3(c) and 3(d), where two different eigenmodes share the same complex eigenvalues and hence experience the same amplifications during evolution.

We note that these degeneracies do not arise from geometric transformations (rotation, reflection, etc.) that leave the network topology invariant but are rather an outcome of hidden symmetries. The nature of these degeneracies can be characterized by a set of operators $\{\hat{A}_i\}$ where $[\hat{H}, \hat{A}_i] = 0$ and $[\hat{A}_i, \hat{A}_j] \neq 0$ [22]. In our system, these operators can be easily identified in the diagonal bases. For example, the diagonal form of $\hat{H}_3^{(2)}$ can be written as $\hat{H}_{D,3}^{(2)} = -\hbar\sqrt{4\kappa^2 - \gamma^2}(\hat{q}_1^\dagger\hat{q}_1 - \hat{q}_3^\dagger\hat{q}_3)$, where $\hat{q}_i^\dagger$ and $\hat{q}_i$ are the creation and annihilation operators associated with the supermodes and as before, the subscript D denotes a diagonal representation. It is now straightforward to show that the operators $\hat{A}_1 = \hat{q}_1^\dagger\hat{q}_2\hat{q}_2\hat{q}_3^\dagger$ and $\hat{A}_2 = \hat{q}_1\hat{q}_2^\dagger\hat{q}_2^\dagger\hat{q}_3$ satisfy the above relations and thus give rise to degeneracy in the spectrum. For example, $\hat{A}_1|0,3,0\rangle_D = |1,1,1\rangle_D$ and $\hat{A}_2|1,1,1\rangle_D = |0,3,0\rangle_D$, while $\hat{A}_1|0,2,1\rangle_D = |1,0,2\rangle_D$ and $\hat{A}_2|1,0,2\rangle_D = |0,2,1\rangle_D$. It is straightforward to see that a similar mathematical analysis applies for higher-order Hamiltonians generated using more iteration. This can be best illustrated by investigating the origin of these degeneracies from a more intuitive perspective. Figure 4 depicts the boson occupation numbers for three pairs of degenerate states associated with the Hamiltonian $\hat{H}_{D,3}^{(2)}$, where the eigenvalue levels (analogous to energy levels in atoms) are shown by yellow thick lines while individual bosons are represented using red spheres. Evidently, these degeneracies arise from the existence of different possible boson distribution profiles that share the same eigenvalue. It is now

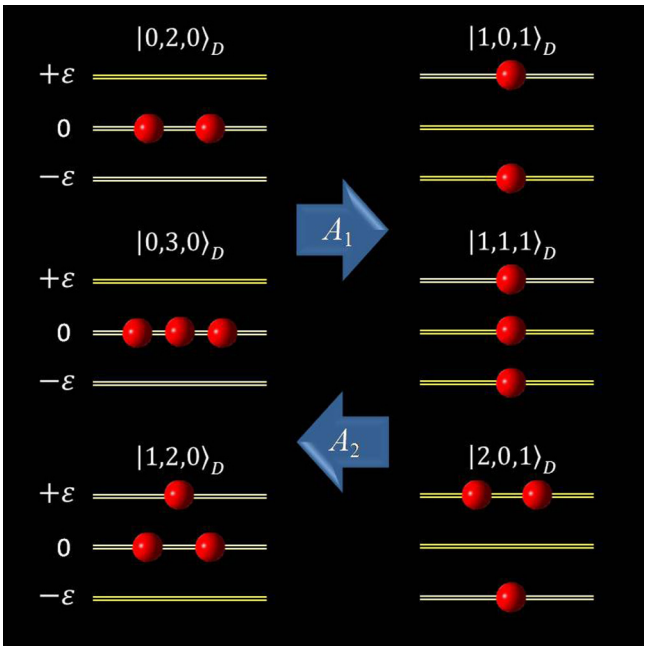

FIG. 4. (Color online) Depicts boson occupation numbers of some degenerate eigenstates (each degenerate pair is schematically shown in one row) associated with the Hamiltonian $\hat{H}^{(2)}_{D,3} = -\varepsilon\,(\hat{q}_1^\dagger \hat{q}_1 - \hat{q}_3^\dagger \hat{q}_3)$, where $\varepsilon = \hbar\sqrt{4\kappa^2 - \gamma^2}$. The eigenvalue levels (analogous to energy levels in atoms) are shown by thick yellow lines, while individual bosons are represented using red spheres. For instance, it is clear that bosonic occupation configurations shown in the first row have a null eigenvalue. The action of hidden symmetry operators $A_{1,2}$ is also indicated in the figure. Evidently, even higher-order degeneracies will arise for Hamiltonians associated with more than three sites.

clear that higher-order Hamiltonians that exhibit more than three "energy" levels will even have more bosonic distribution configurations that share the same eigenvalues, and thus more degeneracies are expected for networks generated by using higher iterations.

This existence of these degeneracies is an intriguing feature that merits further investigation. For example, it would be of interest to investigate the interplay between nonlinear interactions and hidden symmetries on the lasing characteristics of multicavity photonic molecules having similar topologies. We carry these investigations somewhere else.

IV. CONSERVATION LAWS

Next we investigate light transport in these $\mathcal{PT}$-symmetric photonic structures and we study the associated conservation laws. Our numerical analysis indicates that perfect state transfer is possible in these geometries only for certain initial conditions. In order to demonstrate this feature, we plot the evolution of optical field intensities for the configuration shown in Fig. 2(a) in the $\mathcal{PT}$-symmetric phase under two different excitations. Figure 5(a) shows light transport dynamics under the initial condition $c_n(0) = \delta_{n,1}$. Perfect state transfer from c_1 to c_6 (waveguide numbering scheme is depicted in the figure) occurs after a propagation distance l_1. Figure 5(b) shows the full revival cycle associated with Fig. 5(a). Note

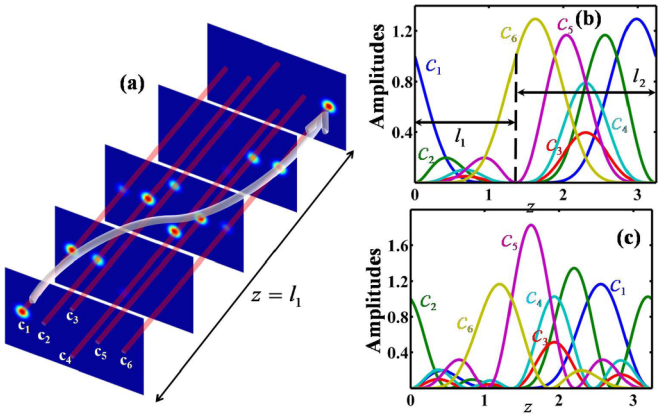

FIG. 5. (Color online) (a) Light transport in the array shown in Fig. 2(a) under the initial excitations: $c_n(0) = \delta_{n,1}$. Note that perfect state transfer from c_1 to c_6 occurs after a propagation distance l_1. (b) Depicts the revival dynamics after one full cycle where coherent transport in the opposite direction (from c_6 to c_1) occurs after $l_1 \neq l_2$. Note that the optical power levels depend on the transport direction. (c) Demonstrates the absence of PST when the initial excitation is $c_n(0) = \delta_{n,2}$. The transparent cylinders in (a) represent the individual waveguides. The array numbering scheme is also indicated in (a).

that coherent transport in the opposite direction (from c_6 to c_1) occurs after a distance $l_2 \neq l_1$. Moreover, the optical power levels depend on the direction of transport (left to right versus right to left). Finally, Fig. 5(c) depicts the same quantities when $c_n(0) = \delta_{n,2}$. Clearly no perfect transfer is observed in this case. This conditional PST in non-Hermitian lattices was also highlighted in [18] in the special case when the propagation distance corresponds to the revival half cycle. In a more general scenario, coherent transport length in non-Hermitian lattices is not necessarily restricted to the evolution half cycle $(l_1 + l_2)/2$.

We now explore the conservation laws associated with light transport in these $\mathcal{PT}$-invariant networks. The simple case of two coupled $\mathcal{PT}$-symmetric waveguides were treated using Stokes parameters [15]. However, these calculations become cumbersome for complicated configurations. Here we present an alternative route for obtaining the system's constants of motion using standard matrix algebra. In quantum mechanics, conservation laws arise from symmetry operators that commute with the Hermitian Hamiltonian. However, for any general non-Hermitian Hamiltonian $\hat{H}$, the conserved quantities Q_i are associated with operators $\hat{S}_i$ that satisfy the relation $\hat{S}_i\hat{H} - \hat{H}^\dagger\hat{S}_i = 0$ and are given by $Q_i = \langle\hat{S}_i\rangle$. For discrete systems, the above operators reduce to matrices, and the conserved quantities can be obtained by solving the above modified commutation relation for the unknown elements of the matrix S_i. To illustrate the expediency of this technique, we consider the $\mathcal{PT}$-symmetric network described by Eq. (3) when $\gamma \neq 0$ and we treat the case of $N = 1$ [Fig. 1(a)]. In this case, the above procedure yields the condition $s_{11} = s_{33}$, where s_{ij} represents that elements of matrix S. Moreover, we find that the linear system of equations is of rank 5 and we choose s_{12}, s_{22}, and s_{32} as free parameters. We then obtain the independent solutions by identifying three different vectors that span the parameter space (s_{12}, s_{22}, s_{32}). One particular

choice of these bases gives

$$S_1 = \begin{bmatrix} 0 & 0 & 1 \\ 0 & 1 & 0 \\ 1 & 0 & 0 \end{bmatrix}, \quad S_2 = \begin{bmatrix} 0 & 1 & i\gamma/\sqrt{2}\kappa \\ 1 & 0 & 1 \\ -i\gamma/\sqrt{2}\kappa & 1 & 0 \end{bmatrix},$$

$$S_3 = \begin{bmatrix} 1 & i\gamma/\sqrt{2}\kappa & -\left(\gamma^2/2\kappa^2+1\right) \\ -i\gamma/\sqrt{2}\kappa & 0 & i\gamma/\sqrt{2}\kappa \\ -\left(\gamma^2/2\kappa^2+1\right) & -i\gamma/\sqrt{2}\kappa & 1 \end{bmatrix}$$

and the associated conserved quantities $Q_{1,2,3} = \vec{c}^{\dagger} S_{1,2,3}\, \vec{c}$ are $Q_1 = (c_1^* c_3 + c_1 c_3^*) + |c_2|^2$, $Q_2 = (c_1^* c_2 + c_1 c_2^*) + (c_3^* c_2 + c_3 c_2^*) + \frac{i\gamma}{\sqrt{2}\kappa}(c_1^* c_3 - c_1 c_3^*)$, and $Q_3 = |c_1|^2 + |c_3|^2 + \frac{i\gamma}{\sqrt{2}\kappa}(c_1^* c_2 - c_1 c_2^*) - \frac{i\gamma}{\sqrt{2}\kappa}(c_3^* c_2 - c_3 c_2^*) - (\frac{\gamma^2}{2\kappa^2}+1)(c_1^* c_3 + c_1 c_3^*)$. Evidently, the above calculation is straightforward and can be generalized to any $\mathcal{PT}$-symmetric network of any complexity and dimensionality.

V. PHOTONIC IMPLEMENTATION

In this section, we discuss several possible implementations of the $\mathcal{PT}$-symmetric networks of Figs. 1 and 2. We note that the structure in Fig. 1 is one dimensional and can be implemented using planar waveguide technology in different material systems. For instance, a possible realization of the fourth-order exceptional point of Fig. 1(b) is shown in Fig. 6(a). In these arrangements, silicate ridge waveguides are fabricated on top of an Er/Yb layer that provides the gain under proper pumping. Recently, the optical properties of 2.4 μm wide and 7.8 mm long Er/Yb silicate strip loaded waveguides have been investigated and experimentally measured [23]. It was shown that these structures can provide up to 5.5 dB of signal amplification at 1530 nm. The coupling constants between waveguides can be controlled by adjusting the distances $d_{1,2}$ and the gradient loss can be achieved by several methods. For example, similar to the work in [11], loss can be introduced through periodic thin metal film stripes [not shown in Fig. 6(a)] with varying duty cycles on top of each waveguide. Another possibility is to imprint diffraction grating on top of the waveguides to provide loss through the coupling to the continuum. The grating parameters will be then designed to provide the exact desired loss for each guiding channel. We note that introducing losses by either one of the aforementioned techniques can perturb the effective index of the guided modes. This effect can be offset by varying the ridge width and/or height.

The implementation of the two-dimensional topologies of Fig. 2 in waveguide systems is more challenging but is still possible through laser writing technology. For example, Taccheo *et al.* have fabricated Er/Yb doped waveguide in a host bulk glass by using femtosecond laser pulses [24]. In these systems, the substrate was made of phosophate glass doped with Er_2O_3 and Yr_2O_3. The operating wavelength was 1533.5 nm and the optical gain was 4 dB. The gradient optical losses in these geometries can be achieved by introducing small curvature in each waveguide channel [25]. Figure 6(b) shows a schematic of such arrangements, where again the distances between waveguides can be engineered to produce the desired coupling coefficients.

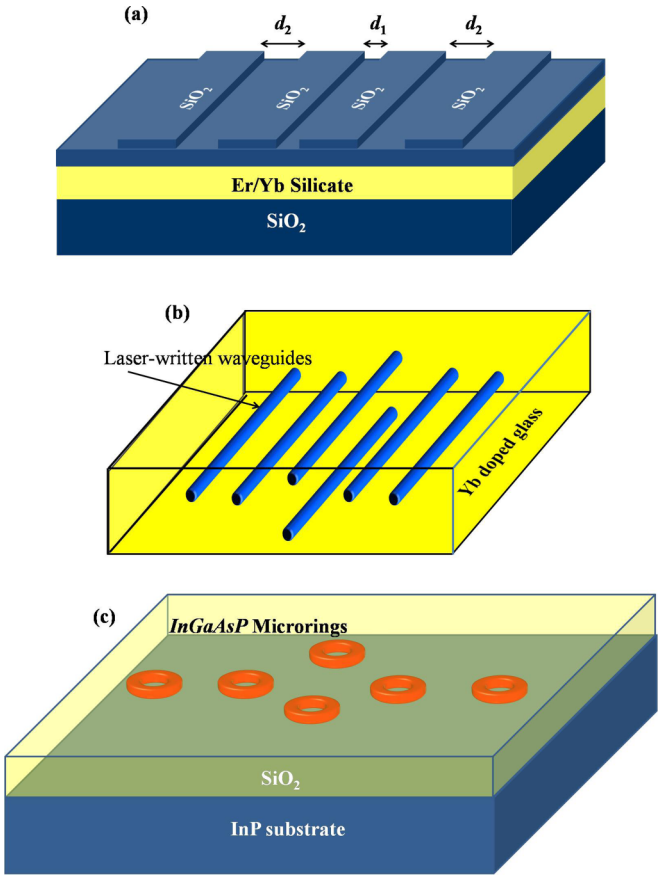

FIG. 6. (Color online) Schematics of possible implementation of $\mathcal{PT}$ networks using (a) Er/Yr planar waveguide technology, (b) two-dimensional Er/Yr laser-written waveguide channels, and (c) semiconductor microring resonators. Details about material systems and principle of operations are presented in the text.

Another more attractive alternative for building the two-dimensional networks of Fig. 2 is by using coupled resonators. Recently, optical resonators made of InGaAsP in silica were employed to realize $\mathcal{PT}$-symmetric lasers [26]. In this study, the widths of the microring resonators were 300 nm and their radii were 5 μm, while the separation between the two rings was taken to be 1 μm to produce a coupling of $\approx 1.3 \times 10^{12}\ \mathrm{s}^{-1}$. The optical gain in this system was achieved by pumping at a wavelength of 1064 nm, while optical loss naturally exists due to the finite quality factor of the optical cavity. Similar structures can be used for building the $\mathcal{PT}$ networks of Figs. 2(a) and 2(b). For illustration purposes, Fig. 6(c) depicts such a possible microring implementation of the structure investigated in Fig. 2(a). Similar to the waveguide scenario, the separation between the resonators is a control design parameter that can be used for tuning the coupling constants between adjacent rings [26]. While in principle, the same strategy can be utilized to implement the $\mathcal{PT}$ network of Fig. 2(b), due to its higher complexity, undesirable cross coupling might present a real obstacle. Under these circumstances, long distance coupling such as demonstrated by Sato *et al.* [27] can provide a solution. In all these microring implementations, gradient loss can be introduced by a judicious deformation of the ring structure to tune the quality factor. Alternatively, one can keep the radiation loss constant and instead vary the optical

gain by controlling the intensity gradient of the pump beam [26]. Finally, we note that other platforms, such as electric circuits [28], for instance, can be also used to implement and experimentally investigate the $\mathcal{PT}$-symmetric networks presented in this work.

VI. CONCLUSION

In conclusion, we have introduced a recursive bosonic quantization technique for generating classical $\mathcal{PT}$ photonic structures that possess hidden symmetries and higher-order exceptional points. We have also investigated the nature of the eigensolutions as well as light transport in these geometries, and we have demonstrated that perfect state transfer is possible only for certain initial conditions. Moreover, we have shown that this coherent transport is asymmetric, with field amplitudes following two different trajectories in opposite transport directions. A general scheme for identifying the conservation laws in such $\mathcal{PT}$-symmetric photonic networks has been also presented.

ACKNOWLEDGMENTS

R.E. would like to thank Dr. K.G. Makris from Vienna University of Technology for useful discussions. The work of D.N.C. was partially supported by NSF (grant ECCS-1128520) and AFOSR (grants FA9550-12-1-0148 and FA9550-14-1-0037).

[1] C. M. Bender and S. Boettcher, Phys. Rev. Lett. **80**, 5243 (1998).
[2] C. M. Bender, Rep. Prog. Phys. **70**, 947 (2007).
[3] A. Znojil, Phys. Lett. A **285**, 7 (2001).
[4] Z. Ahmed, Phys. Lett. A **282**, 343 (2001).
[5] W. D. Heiss, M. Müller, and I. Rotter, Phys. Rev. E **58**, 2894 (1998).
[6] W. D. Heiss, J. Phys. A: Math. Gen. **37**, 2455 (2004)
[7] R. El-Ganainy, K. G. Makris, D. N. Christodoulides, and Z. H. Musslimani, Opt. Lett. **32**, 2632 (2007).
[8] K. G. Makris, R. El-Ganainy, D. N. Christodoulides, and Z. H. Musslimani, Phys. Rev. Lett. **100**, 103904 (2008).
[9] Z. H. Musslimani, K. G. Makris, R. El-Ganainy, and D. N. Christodoulides, Phys. Rev. Lett. **100**, 030402 (2008).
[10] K. G. Makris, R. El-Ganainy, D. N. Christodoulides, and Z. H. Musslimani, Phys. Rev. A **81**, 063807 (2010).
[11] A. Guo, G. J. Salamo, D. Duchesne, R. Morandotti, M. Volatier-Ravat, V. Aimez, G. A. Siviloglou, and D. N. Christodoulides, Phys. Rev. Lett. **103**, 093902 (2009).
[12] C. E. Ruter, K. G. Makris, R. El-Ganainy, D. N. Christodoulides, M. Segev, and D. Kip, Nat. Phys. **6**, 192 (2010).
[13] Z. Lin, H. Ramezani, T. Eichelkraut, T. Kottos, H. Cao, and D. N. Christodoulides, Phys. Rev. Lett. **106**, 213901 (2011).
[14] F. Nazari, N. Bender, H. Ramezani, M. K. Moravvej-Farshi, D. N. Christodoulides, and T. Kottos, arXiv:1310.2313.
[15] H. Ramezani, T. Kottos, R. El-Ganainy, and D. N. Christodoulides, Phys. Rev. A **82**, 043803 (2010).
[16] A. P. Perez-Leija, R. Keil, A. Kay, H. Moya-Cessa, S. Nolte, L.-C. Kwek, B. M. Rodríquez-Lara, A. Szameit, and D. N. Christodoulides, Phys. Rev. A **87**, 012309 (2013).
[17] E. M. Graefe, U. Günther, H. J. Korsch and A. E. Niederle, J. Phys. A: Math. Theor. **41**, 255206 (2008).
[18] X. Z. Zhang, L. Jin, and Z. Song, Phys. Rev. A **85**, 012106 (2012).
[19] A. Regensburger, C. Bersch, M. A. Miri, G. Onishchukov, D. N. Christodoulides, and U. Peschel, Nature (London) **488**, 167 (2012).
[20] T. Eichelkraut, R. Heilmann, S. Weimann, S. Stützer, F. Dreisow, D. N. Christodoulides, S. Nolte, and A. Szameit, Nat. Commun. **4**, 2533 (2013).
[21] B. Peng, S. K. Ozdemir, F. Lei, F. Monifi, M. Gianfreda, G. L. Long, S. Fan, F. Nori, C. M. Bender, and L. Yang, Nat. Phys. **10**, 394 (2014).
[22] E. A Yuzbashyan, W. Happer, B. L Altshuler, and S. B Shastry, J. Phys. A: Math. Gen. **36**, 2577 (2003).
[23] R. Guo, X. Wang, K. Zang, B. Wang, L. Wang, L. Gao, and Z. Zhou, Appl. Phys. Lett. **99**, 161115 (2011).
[24] S. Taccheo, G. Della Valle, R. Osellame, G. Cerullo, N. Chiodo, P. Laporta, O. Svelto, A. Killi, U. Morgner, M. Lederer, and D. Kopf, Opt. Lett. **29**, 2626 (2004).
[25] J. M. Zeuner, M. C. Rechtsman, Y. Plotnik, Y. Lumer, M. S. Rudner, M. Segev, and A. Szameit, arXiv:1408.2191.
[26] H. Hodaei, M.-A. Miri, M. Heinrich, D. N. Christodoulides, and M. Khajavikhan, arXiv:1405.2103.
[27] Y. Sato, Y. Tanaka, J. Upham, Y. Takahashi, T. Asano, and S. Noda, Nat. Photon. **6**, 56 (2012).
[28] J. Schindler, A. Li, M. C. Zheng, F. M. Ellis, and T. Kottos, Phys. Rev. A **84**, 040101(R) (2011).